(c)2001 American Institute of Aeronautics & Astronautics or Published with Permission of Author(s) and/or Author(s)' Sponsoring Organization.

A01-16820

AIAA-00-1029

Monte Carlo Computations of Hypersonic Interacting Flows

I. D. Boyd and W.-L. Wang
University of Michigan
Ann Arbor, MI 48109.

39th AIAA Aerospace Sciences Meeting & Exhibit
8-11 January 2001 / Reno, NV

For permission to copy or republish, contact the American Institute of Aeronautics and Astronautics
1801 Alexander Bell Drive, Suite 500, Reston, VA 20191

(c)2001 American Institute of Aeronautics & Astronautics or Published with Permission of Author(s) and/or Author(s)' Sponsoring Organization.

MONTE CARLO COMPUTATIONS OF HYPERSONIC INTERACTING FLOWS

Iain D. Boyd* and Wen-Lan Wang†

University of Michigan, Ann Arbor, MI 48109

Abstract

Computations using the direct simulation Monte Carlo (DSMC) method are presented for hypersonic flows about hollow–cylinder/flare and double–cone configurations. These computations are part of a code validation exercise. The flow conditions are in the near-continuum regime making the computations very expensive numerically. Several million particles and long run times are required. Indeed, the results presented here have not yet reached steady state despite consuming large quantities of run time. The results do indicate qualitatively the expected phenomena, such as flow separation, but it is anticipated that these structures are not yet fully resolved due to the inadequate amount of physical time that has been simulated. It is concluded that substantially larger computer resources are required in order to apply DSMC successfully to these types of flows.

Introduction

There is significant interest around the world in the development of hypersonic vehicles for access to space. Due to the tremendous technical difficulties and costs in obtaining laboratory and flight measurements under realistic conditions, a great deal of emphasis will be placed on the role of computational modeling in the design of new hypersonic vehicles. The study reported in this paper is a component of a hypersonic code validation exercise organized by Dr. Michael Holden. The exercise consists of several well documented laminar, non-reacting test cases that are among many that have been tested experimentally in the hypersonic facilities at CUBRC.[1] The test cases were designed to involve flow phenomena that are relevant to hypersonic vehicle design and that provide a challenge for computational models. The three basic geometric configurations are: (1) a cylinder with flare; (2) a double cone; and (3) an oblique shock impinging on a cylinder.

In this paper, we describe results obtained using the direct simulation Monte Carlo method (DSMC)[2] for configurations (1) and (2). The cylinder–flare geometry has been investigated at lower enthalpy using the DSMC technique by Markelov et al.[3] and by Moss.[4] Moss[5] has also analyzed cone–cone flows very similar to those considered here using the DSMC method. The particular flow conditions considered are listed in Tables 1 and 2. The overall Knudsen numbers for these flows are based on a hard sphere mean free path and characteristic lengths of 0.1017 and 0.092 m for the cylinder–flare and cone–cone flows, respectively. These values are the lengths of the cylinder and the first cone, respectively. The Knudsen numbers are very small

* Associate Professor. Department of Aerospace Engineering. Senior Member AIAA

† Graduate Student Research Assistant. Department of Aerospace Engineering

(c)2001 American Institute of Aeronautics & Astronautics or Published with Permission of Author(s) and/or Author(s)' Sponsoring Organization.

from the perspective of the DSMC technique. However, there is considerable interest in obtaining DSMC solutions for these flows because previous continuum computations (solving the Navier-Stokes equations with coupled thermo-chemistry) at high enthalpy were in poor agreement with experimental measurements.[6,7] Several suggestions have been made to explain the inaccuracy of the continuum results including unsteady flow, three-dimensional flow, and non-continuum effects due to the very steep gradients in flow field properties as well as the possibility of wall slip phenomena.

The layout of the paper is as follows. First, a detailed description is provided of the particular DSMC code employed in this study. Then, results are presented and discussed for the double cone studies. Finally, the results for the cylinder–flare configuration are presented.

The DSMC Code MONACO

MONACO is a general, object-oriented, cell-based, parallelized implementation of the DSMC method first developed by Dietrich and Boyd[8] in 1996. In the original code, a mixture of FORTRAN (for floating point operations) and C (for memory management) was employed. Parallelization is performed using domain decomposition. In the original study,[8] a 400-processor computation on the first IBM SP-2 super-computer was performed on MONACO using 100 million particles. Since that time, MONACO has been further developed and applied to a range of rarefied gas problems including three-dimensional spacecraft plume studies,[9] spacecraft glow modeling,[10] thin film deposition,[11,12] and meteoroid trail analysis.[13]

MONACO employs the Variable Soft Sphere (VSS) collision model,[14] the variable rotational energy exchange probability model of Boyd,[15] and the variable vibrational energy exchange probability model of Vijayakumar et al..[16] The flow conditions here do not involve chemical reactions. Simulation of the interactions of the particles with the walls employs accommodation and momentum reflection coefficients of 0.85.

MONACO offers a great deal of control over the numerical parameters employed in a simulation. Both unstructured triangular, or structured rectangular cells may be employed in two-dimensional simulations. Cell weighting factors and time-steps may be set uniquely for each cell in the grid. A sub-cell system is implemented for selection of collision pairs where the number of sub-cells is scaled by the local mean free path.

Cylinder–Flare Studies

As indicated in Table 1, we consider CUBRC Case 11 which involves the extended flare. As shown in Fig. 1, a regular, structured grid consisting of 2,000 cells along the body by 400 cells normal to the body is employed. The grid begins at a small distance in front of the leading edge of the hollow cylinder. Sub-cells are also employed with the number in each direction based on the local mean free path. A reference time step of 5×10^{-9} sec is employed. A total number of 4 million particles is employed. The final results presented below are obtained by sampling over the period from 1.0 to 1.1 msec. At the end of this interval, it is clear

(c)2001 American Institute of Aeronautics & Astronautics or Published with Permission of Author(s) and/or Author(s)' Sponsoring Organization.

that the results have not yet reached steady state. These calculations are obtained by running for four days on 16 IBM-SP processors at a parallel efficiency of about 90%.

A general impression of the complex flow field can be obtained from Figs. 2a and 2b that show contours of number density ratio (n/n_∞) and translational temperature (K), respectively. In the region vertically above the cylinder, the number density is reduced by a factor of about 5 from the free stream value. The gas is subsequently compressed to values in excess of 6 times the free stream by the flare. The regions of lower and higher pressure above the cylinder and flare, respectively, combine to generate a complex flow interaction that includes flow separation and re-attachment on either side of the compression corner. The temperature is increased in the region above the cylinder due to viscous interaction with a peak value less than 1,000 K. The strong compression caused by the flare leads to further heating with peak values of about 1,500 K reached above the flare.

To discuss the physical properties of the solution in detail, data has been extracted vertically along three different x-coordinates: x/L=0.5, 1.0, and 1.5 (where L=0.1017 m is the length of the hollow cylinder). In Fig. 3a, the number density is shown. The dramatic decrease in density due to viscous interaction at x/L=0.5, 1.0 can be seen clearly. In the region above the flare, the density rises to a value of about six and then is increased further by the relatively cold wall. In Fig. 3b, profiles of translational temperature are shown. These illustrate the systematic increase in peak translational temperature with horizontal distance.

Surface profiles of friction, pressure and heat transfer coefficients are shown in Figs. 4a–4c, respectively. The most interesting of these is the friction coefficient shown in Fig. 4a. A small separation region is predicted with a horizontal length Δx=0.022 m. This is about 20% smaller than the value of Δx=0.027 m predicted by Moss[4] for the same geometry but slightly different flow conditions (n_∞=1.46 m^{-3}, U_∞=2782 m/s, T_∞=194 K). It is not clear at this point whether the difference in the size of the separation zones is due to the small change in flow conditions or to numerical effects. The surface pressure and heat transfer data show the expected behavior and are consistent with the small region of separation. All the surface properties show a rapid increase at the leading edge of the cylinder. Similar effects are found in the cylinder–flare DSMC computations of Markelov et al.[3] and are due to the assumption of incomplete surface accommodation.

Now, some numerical aspects of the solution are considered along the same vertical lines employed in Figs. 3. In Fig. 5a, the number of simulated particles per cell is shown. Due to the use of geometric weighting factors in the simulation, these profiles mostly follow those for the number density as shown in Fig. 3a. It is clear that a relatively small number of particles-per-cell (in the range of 3 to 6) is employed in the region just above the hollow cylinder. This is the region of minimum number density, and hence maximum mean free path. Hence, the collision rate in this region is a minimum and so the low number of particles is not expected to represent any problem. In Fig. 5b, the ratio of the local mean time between collisions (τ) to the simulation time step (a constant in these studies) is shown. Separation of particle motion and particle collisions in the DSMC method requires that this ratio always be greater than 1. It is clear that this criterion is satisfied everywhere and in fact the profiles suggest that the time step can be increased significantly in the region

(c)2001 American Institute of Aeronautics & Astronautics or Published with Permission of Author(s) and/or Author(s)' Sponsoring Organization.

above the cylinder. In Fig. 5c, the ratio of the computational cell size in the direction of maximum pressure gradient over the local mean free path (λ) is shown. Neglecting particle position within a cell in selecting candidate collision partners in the DSMC method requires that this ratio be less than 1. This criterion is generally satisfied except in the shock front and along the flare where the local cell size is as much as 3 λ. However, this is also the region where there are a large number of particles-per-cell (Fig. 5a) and use of the sub-cell scheme should provide adequate spatial resolution of the collision rate.

In Figs. 6a–6c, the variation along the body surface of these same numerical parameters is shown. In Fig. 6a, it is shown that the number of particles per cell varies from 3 to 100. The variation of the ratio $\tau/\Delta t$ (Fig. 6b) indicates that the criterion of $\tau/\Delta t > 1$ is satisfied everywhere. Finally, the variation of the ratio $\Delta s/\lambda$ (Fig. 6c) shows that the criterion of $\Delta s/\lambda < 1$ is satisfied everywhere.

Double Cone Studies

As indicated in Table 2, we consider CUBRC cases 28 and 35 that involve the two sharp cones with half angles of 25° and 55°. The computational grid employed for Case 28 consists of 2048 cells along the body by 512 cells normal to the body. This grid is plotted in Fig. 7 where again only one in every ten cells is shown in each direction. The base time step for this simulation is 10^{-9} sec although this is decreased in regions of very high density. The solutions shown here are obtained using about 6.4 million particles and averaged over a sampling interval of 0.25 msec to 0.28 msec. At this time, the solution had not yet reached steady state. In particular, the size of the separation region is still growing, although very slowly. These results are obtained by running for 4 days on 16 IBM-SP processors at a parallel efficiency of about 90%.

The same sets of data shown for the cylinder–flare configuration are considered here. In Figs. 8a and 8b, contours of number density ratio (n/n_∞) and translational temperature (K) are shown, respectively. These show the complex shock interaction structure above the intersection of the two cones and the expansion fan at the base of the second cone.

Figures 9a and 9b show vertical profiles of these physical properties at locations of x/L=0.5, 1.0, and 1.5 where L=0.092 m is the length of the first cone. These data are relatively uninteresting and show the increasing shock strength with increasing x/L.

The surface properties are shown in Figs. 10a–10c. There is a lot of structure in these data. Figure 10a indicates a separation region with a horizontal length Δx=0.022 m. The separation shock accompanying this structure gives rise to the sudden increase in pressure and decrease in heat flux at about x=0.08 m, as shown in Figs. 10b and 10c, respectively. Under almost identical flow conditions (n_∞=1.46 m^{-3}, U_∞=2714 m/s, T_∞=194 K), Moss[5] computed a separation zone of Δx=0.0198 m.

Variation of the numerical parameters along the same vertical paths used in Figs. 9 are shown in Figs. 11a–11c. In Fig. 11a, it is shown that the number of particles per cell is generally greater than 10 except in the free stream region. The ratio τ / Δt (Fig. 11b) indicates that the requirement of τ / Δt > 1 is satisfied everywhere. Note, that Δt=10^{-9} sec in all these plots. However, Fig. 11c indicates that the

(c)2001 American Institute of Aeronautics & Astronautics or Published with Permission of Author(s) and/or Author(s)' Sponsoring Organization.

requirement of $\Delta s \ / \ \lambda < 1$ is not satisfied. The failure to meet this criterion grows worse with increasing x/L reaching peak values of 8–10.

To further characterize the behavior of the numerical parameters, their variations along the body surface are shown in Figs. 12a–12c. From Fig. 12a, it is clear that the number of particles per cell is always large along the cone surfaces. In Fig. 12b, it is shown that the ratio $\tau \ / \ \Delta t$ drops significantly at about x/L=0.1 m but even there remains greater than one. It is in this region that the local time-step is reduced from the reference value (10^{-9} sec) by a factor of about two. In Fig. 12c, the ratio $\Delta s \ / \ \lambda$ is below 1 for most of the body, but reaches a maximum at x/L=0.1 m with a value of about 4. The use of sub-cells in these region of maximum numbers of particles per cell should provide adequate spatial resolution of the collision phenomena.

The results for Case 35 are very similar to those obtained for Case 28 and so we show only the surface profiles in Figs. 13. These indicate a smaller separation region of Δx=0.014 m. Once again it is anticipated that this is significantly smaller than the experimental measurements due to the computation not having reached steady state.

Conclusions

It is somewhat difficult to draw firm conclusions from this study prior to the full comparisons of these results with the experimental data and the other numerical solutions submitted in this code validation exercise. However, two things are immediately clear from our experience in trying to compute these flows. Firstly, simulation using the DSMC technique of these types of flow conditions requires very large amounts of computational resources. Our computation of about 0.3 msec of physical time for the Case 28 double cone flow consumed 4 full days of 16 processors of an IBM-SP computer. That is equivalent to two months of single-processor CPU time. The experiments have test times on the order of 3 msec so more than 18 months of single processor time are required. This is well beyond the resources available in our research.

The second conclusion we draw from our results is that the DSMC method appears to predict qualitatively the structure of flow separation that has been seen in prior CFD calculations. However, the size of the separation zones shown here are expected to under-predict those measured experimentally (and possibly predicted by CFD and larger DSMC computations).

Acknowledgments

Funding for this work was provided by the Air Force Office of Scientific Research under grant F49620-01-1-0003 with Dr. Steven Walker as technical monitor. The authors express their gratitude to Graham Candler and Yanni Nompelis of the University of Minnesota for all their assistance in making these computations. Computer resources on the IBM-SP machine at the Minnesota Supercomputing Institute are gratefully acknowledged.

(c)2001 American Institute of Aeronautics & Astronautics or Published with Permission of Author(s) and/or Author(s)' Sponsoring Organization.

References

[1] Holden, M. S., "Experimental Database from CUBRC Studies in Hypersonic Laminar and Turbulent Interacting Flows Including Flowfield Chemistry," CUBRC Report, June 2000.

[2] Bird, G. A., *Molecular Gas Dynamics and the Direct Simulation of Gas Flows*, Oxford University Press, Oxford, 1994.

[3] Markelov, G. N., Kudryatsev, A. N., and Ivanov, M. S., "Continuum and Kinetic Simulation of Laminar Separated Flow at Hypersonic Speeds," *Journal of Spacecraft and Rockets*, Vol. 37, 2000, pp. 499–506.

[4] Moss, J. N., "DSMC Simulation of Separated Flows About Flared Bodies at Hypersonic Conditions," European Congress on Computational Methods in Applied Sciences and Engineering, Barcelona, Spain, September 2000.

[5] Moss, J. N., "DSMC Simulations of Shock Interactions About Sharp Double Cones," NASA TM-2000-210318, August 2000.

[6] Olejniczak, J., Candler, G. V., and Hornung, H. G., "Computation of Double-Cone Experiments in High Enthalpy Nitrogen," AIAA Paper 97-2549, June 1997.

[7] Olejniczak, J., candler, G. V., Wright, M. J., Levya, I. and Hornung, H. G., "An Experimental and Computational Study of High Enthalpy Double-Wedge Flows," *Journal of Thermophysics and Heat Transfer*, Vol. 13, 1999, pp. 431-440.

[8] Dietrich, S. and Boyd, I. D., "Scalar Optimized Parallel Implementation of the Direct Simulation Monte Carlo Method," *Journal of Computational Physics*, Vol. 126, 1996, pp. 328-342.

[9] Kannenberg, K. C. and Boyd, I. D., "Three Dimensional Monte Carlo Simulations of Plume Impingement," *Journal of Thermophysics and Heat Transfer*, Vol. 13, 1999, pp. 226-235.

[10] Karipides, D. P., Boyd, I. D. and Caledonia, G. E., "Detailed Simulation of Surface Chemistry Leading to Spacecraft Glow," *Journal of Spacecraft and Rockets*, Vol. 36, 1999, pp. 566-572.

[11] Chen, G., Boyd, I. D., Roadman, S., and Engstrom J. R., "Monte Carlo Simulation of a Hyperthermal Silicon Deposition Process," *Journal of Vacuum Science and Technology A*, Vol. 16, 1998, pp. 689-699.

[12] Balakrishnan, J., Boyd, I. D., and Braun, D. G., "Monte Carlo Simulation of Vapor Transport in Physical Vapor Deposition of Titanium," *Journal of Vacuum Science and Technology A*, Vol. 18, 2000, pp. 907-916.

[13] Boyd, I. D., "Computation of Atmospheric Entry Flow About a Leonid Meteoroid," *Earth, Moon, and Planets*, Vol. 82, 2000, pp. 93-108.

[14] Koura, K. and Matsumoto, H., "Variable Soft Sphere Molecular Model for Air Species," *Physics of Fluids A*, Vol. 4, 1992, pp. 1083–1085.

[15] Boyd, I. D., "Analysis of Rotational Nonequilibrium in Standing Shock Waves of Nitrogen," *AIAA Journal*, Vol. 28, 1990, pp. 1997-1999.

[16] Vijayakumar, P., Sun, Q. and Boyd, I. D., "Detailed Models of Vibrational-Translational Energy Exchange for the Direct Simulation Monte Carlo Method," *Physics of Fluids*, Vol. 11, 1999, pp. 2117-2126.

(c)2001 American Institute of Aeronautics & Astronautics or Published with Permission of Author(s) and/or Author(s)' Sponsoring Organization.

Table 1. Flow conditions for the cylinder–flare studies.

CUBRC Case Number[1]	n_∞ (m^{-3})	U_∞ (m/s)	T_∞ (K)	Kn_∞
11	1.09×10^{22}	2609	129	1.3×10^{-3}

Table 2. Flow conditions for the double cone studies.

CUBRC Case Number[1]	n_∞ (m^{-3})	U_∞ (m/s)	T_∞ (K)	Kn_∞
28	1.41×10^{22}	2664	186	1.1×10^{-3}
35	1.19×10^{22}	2713	139	1.3×10^{-3}

(c)2001 American Institute of Aeronautics & Astronautics or Published with Permission of Author(s) and/or Author(s)' Sponsoring Organization.

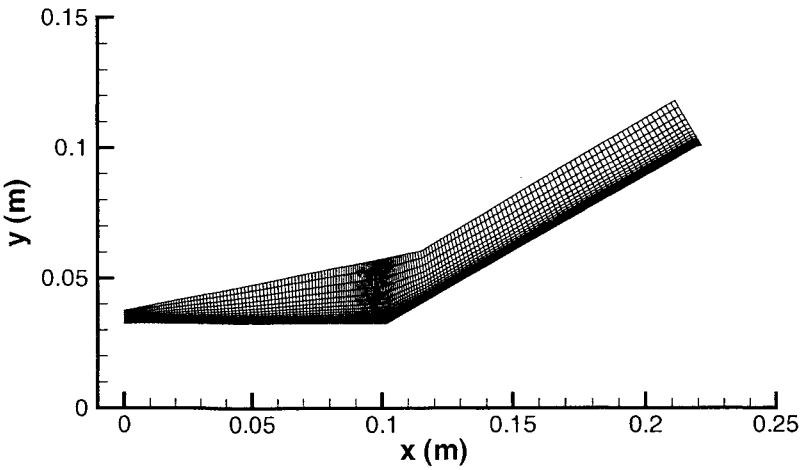

Fig. 1. Grid employed for cylinder-flare Case 11 (1 in 10 points shown in each direction).

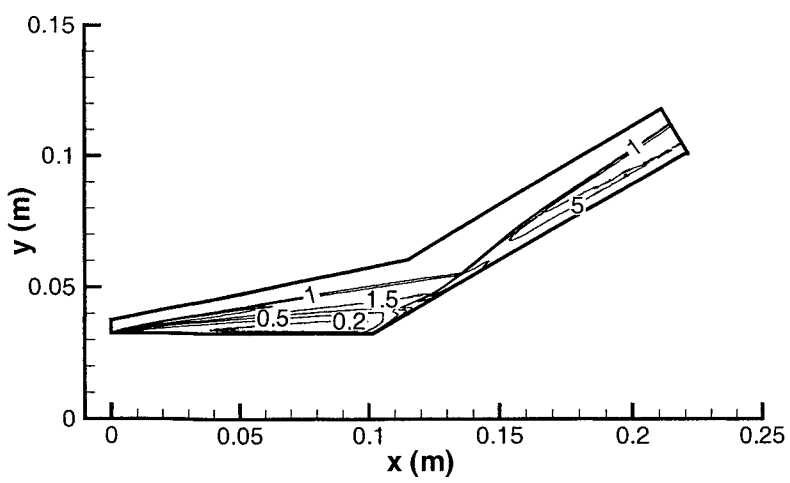

Fig. 2a. Contours of number density ratio (n/n_∞).

(c)2001 American Institute of Aeronautics & Astronautics or Published with Permission of Author(s) and/or Author(s)' Sponsoring Organization.

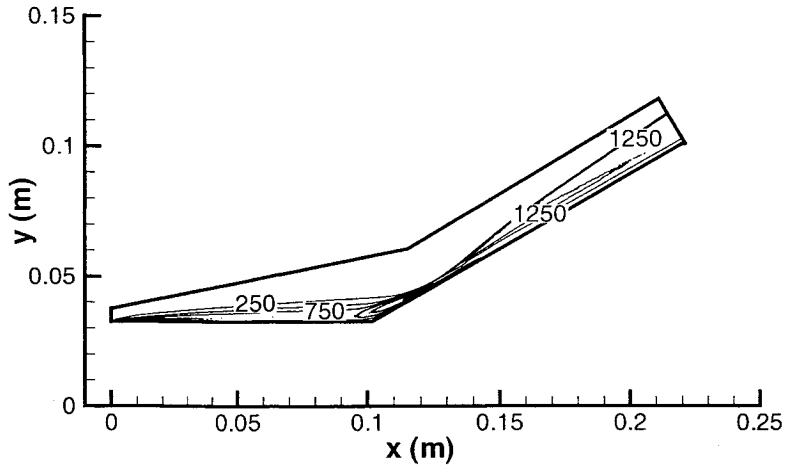

Fig. 2b. Contours of translational temperature (K).

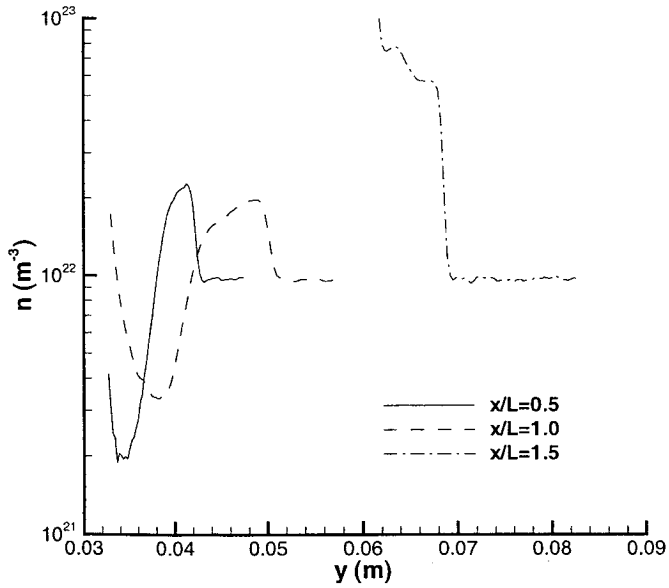

Fig. 3a. Profiles of number density along three different constant-x coordinates.

(c)2001 American Institute of Aeronautics & Astronautics or Published with Permission of Author(s) and/or Author(s)' Sponsoring Organization.

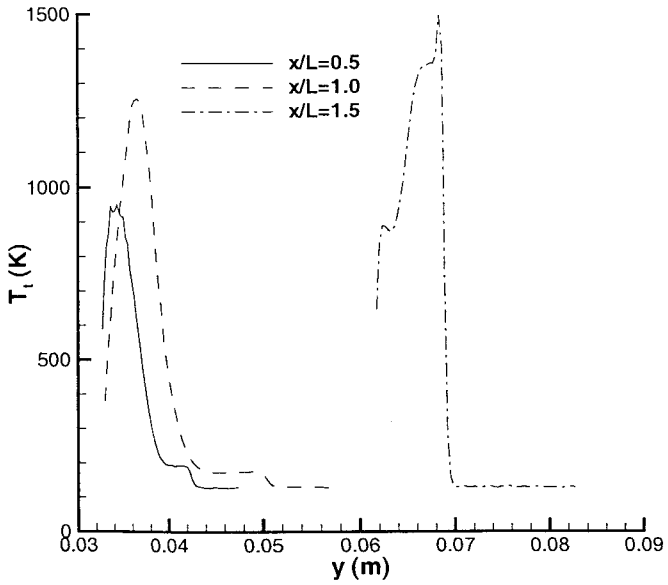

Fig. 3b. Profiles of translational temperature along three different constant-x coordinates.

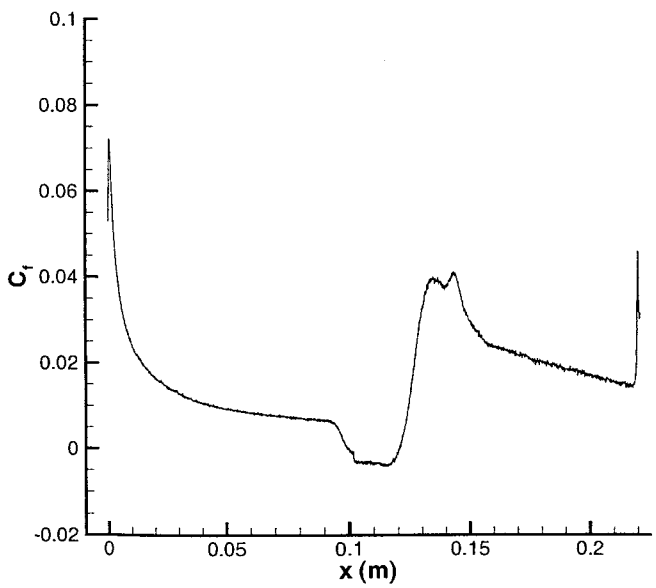

Fig. 4a. Surface profile of friction coefficient.

(c)2001 American Institute of Aeronautics & Astronautics or Published with Permission of Author(s) and/or Author(s)' Sponsoring Organization.

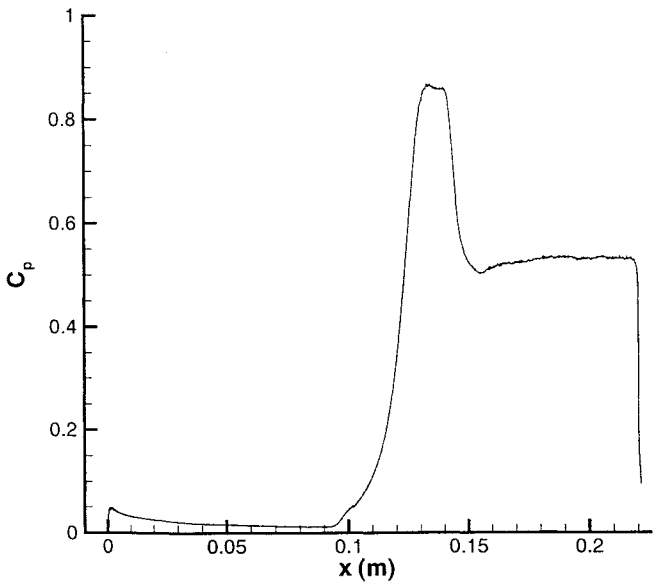

Fig. 4b. Surface profile of pressure coefficient.

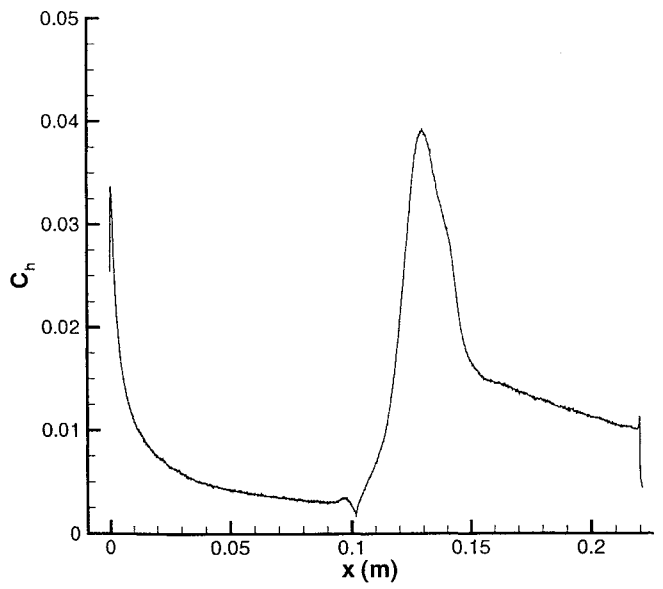

Fig. 4c. Surface profile of heat transfer coefficient.

(c)2001 American Institute of Aeronautics & Astronautics or Published with Permission of Author(s) and/or Author(s)' Sponsoring Organization.

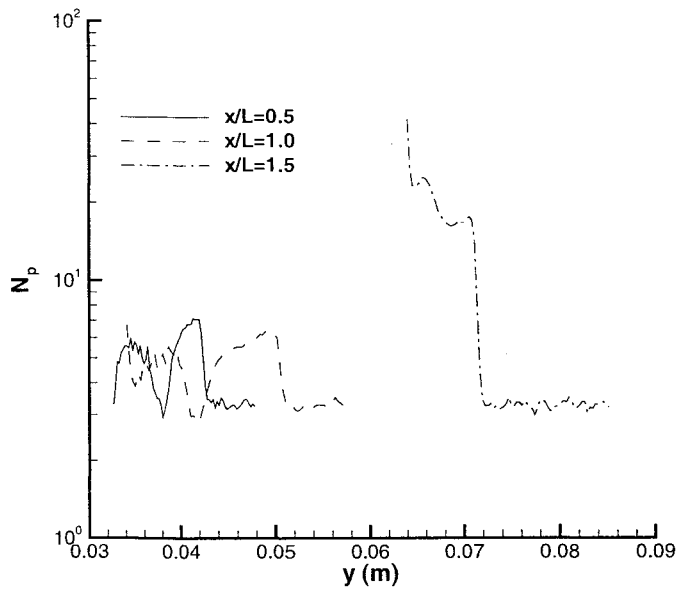

Fig. 5a. Number of particles per cell along three different constant-x coordinates.

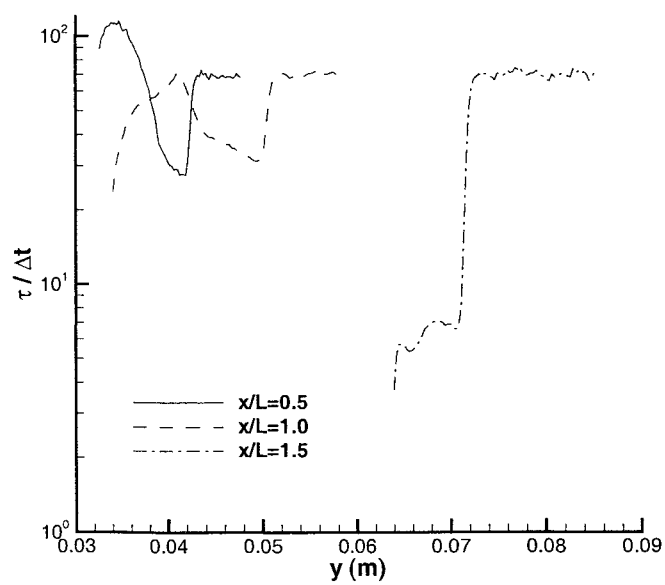

Fig. 5b. Ratio of local mean free time to the simulation time-step along three different constant-x coordinates.

(c)2001 American Institute of Aeronautics & Astronautics or Published with Permission of Author(s) and/or Author(s)' Sponsoring Organization.

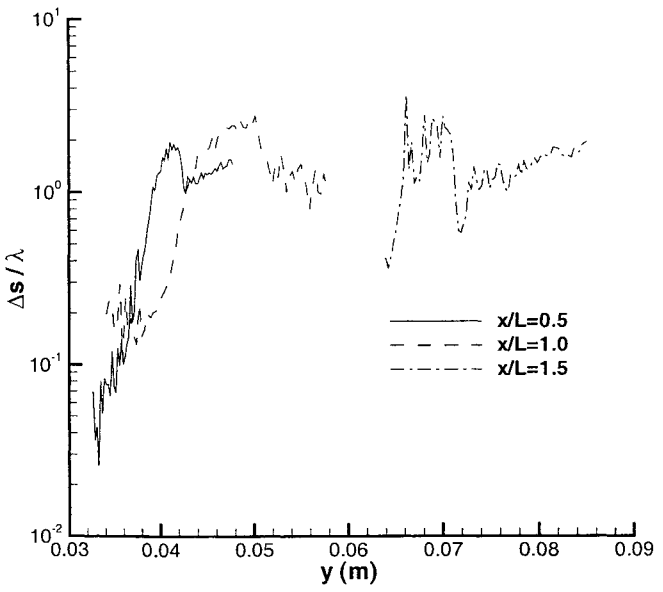

Fig. 5c. Ratio of simulation cell size in direction of maximum gradient to local mean free path along three different constant-x coordinates.

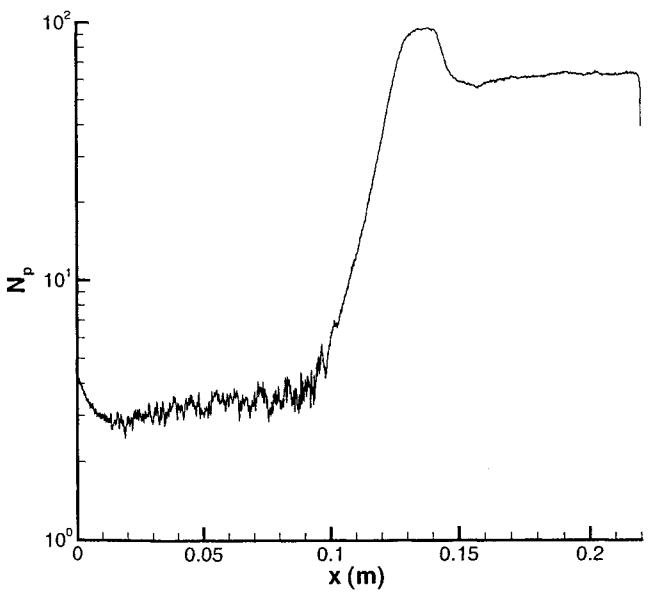

Fig. 6a. Number of particles per cell along the body surface.

(c)2001 American Institute of Aeronautics & Astronautics or Published with Permission of Author(s) and/or Author(s)' Sponsoring Organization.

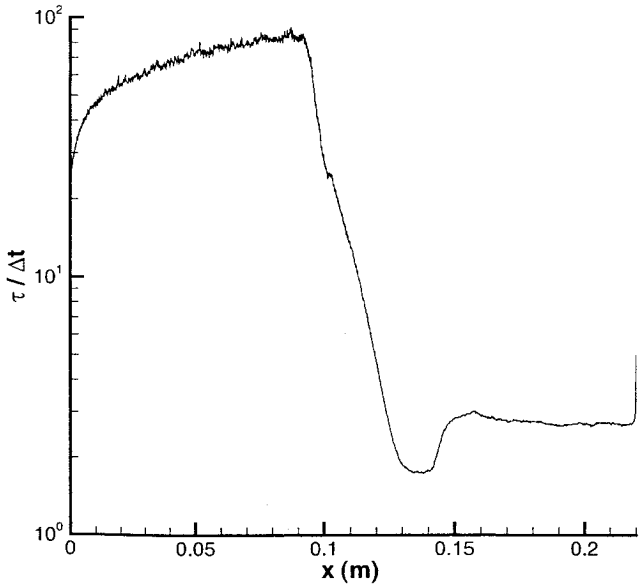

Fig. 6b. Ratio of local mean free time to the simulation time-step along the body surface.

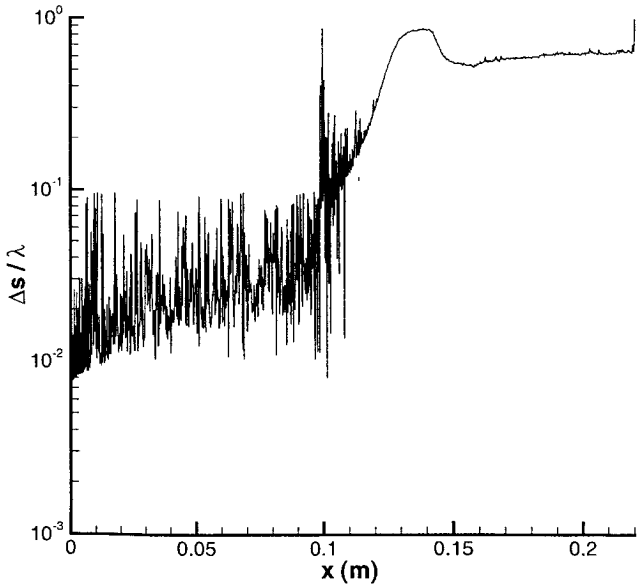

Fig. 6c. Ratio of simulation cell size in direction of maximum gradient to local mean free path along the body surface.

(c)2001 American Institute of Aeronautics & Astronautics or Published with Permission of Author(s) and/or Author(s)' Sponsoring Organization.

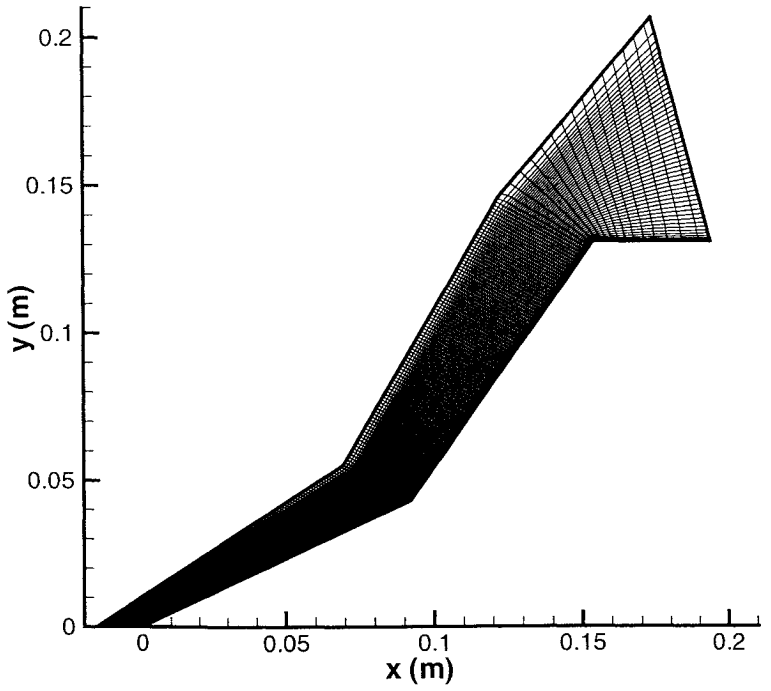

Fig. 7. Grid employed for cone-cone Case 28 (1 in 10 points shown in each direction).

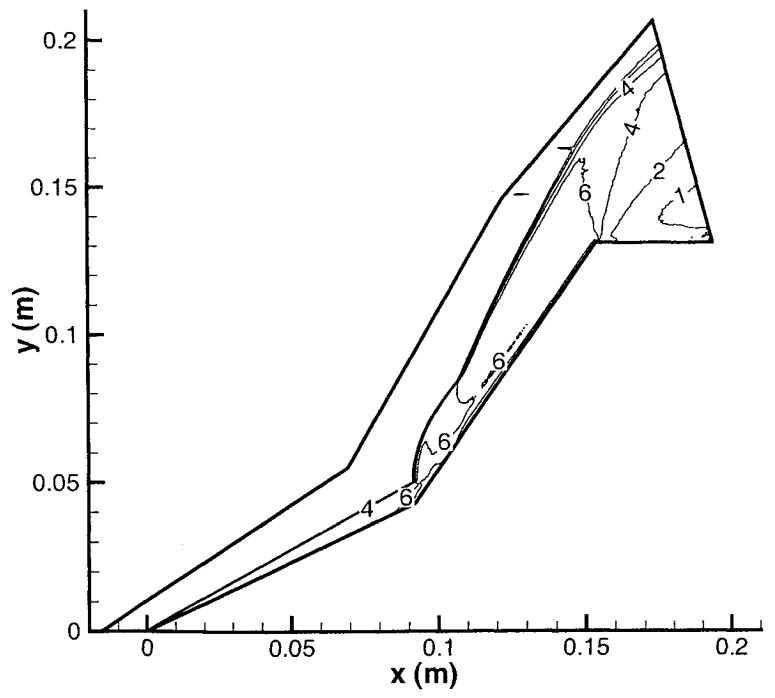

Fig. 8a. Contours of number density ratio (n/n_∞).

(c)2001 American Institute of Aeronautics & Astronautics or Published with Permission of Author(s) and/or Author(s)' Sponsoring Organization.

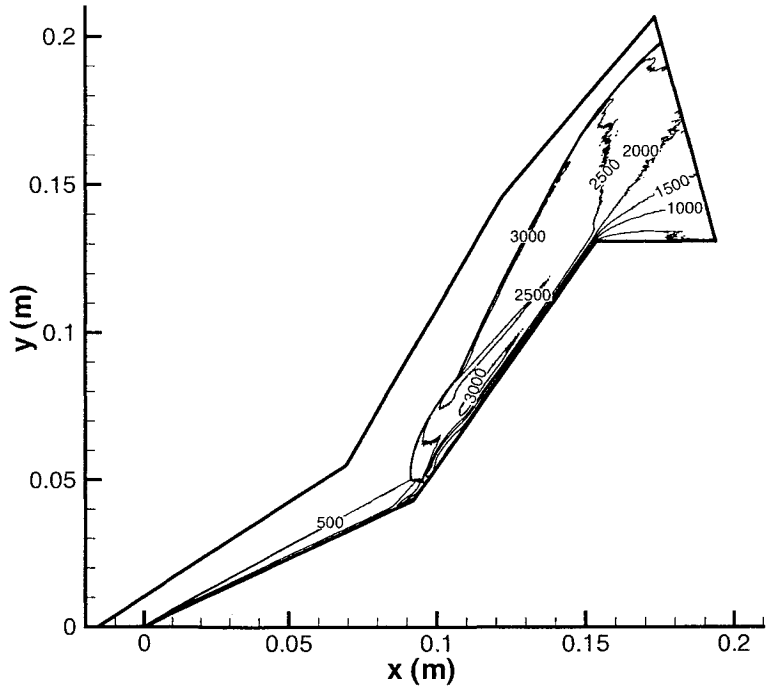

Fig. 8b. Contours of translational temperature (K).

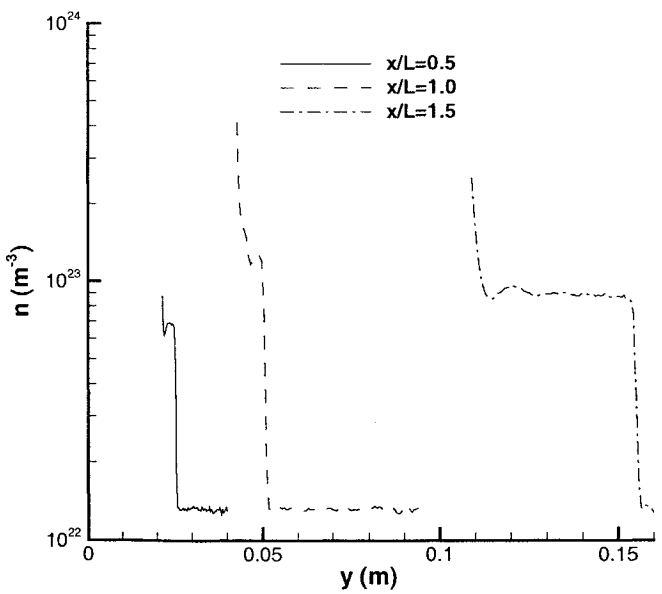

Fig. 9a. Profiles of number density along three different constant-x coordinates.

(c)2001 American Institute of Aeronautics & Astronautics or Published with Permission of Author(s) and/or Author(s)' Sponsoring Organization.

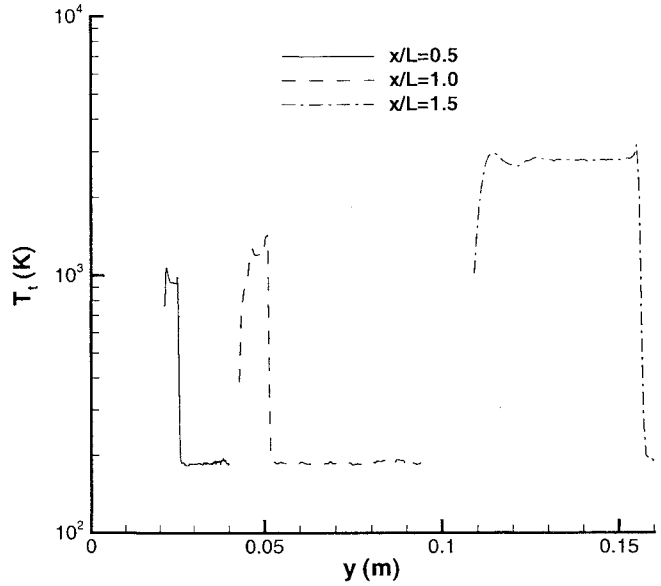

Fig. 9b. Profiles of translational temperature along three different constant-x coordinates.

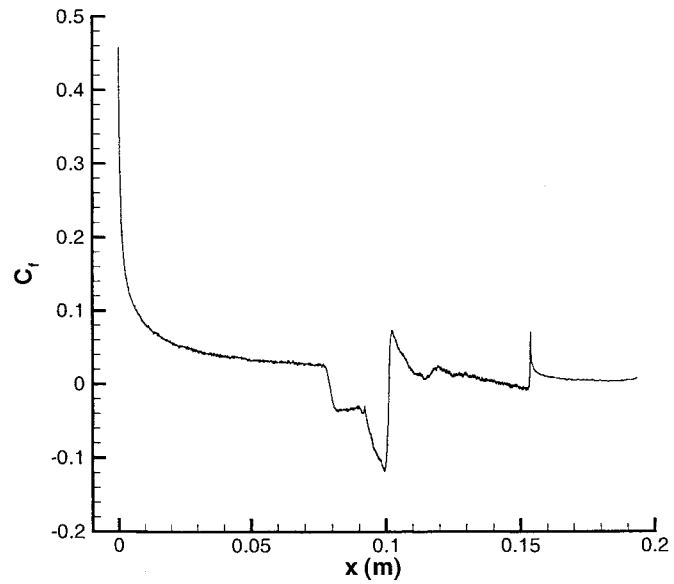

Fig. 10a. Surface profile of friction coefficient.

(c)2001 American Institute of Aeronautics & Astronautics or Published with Permission of Author(s) and/or Author(s)' Sponsoring Organization.

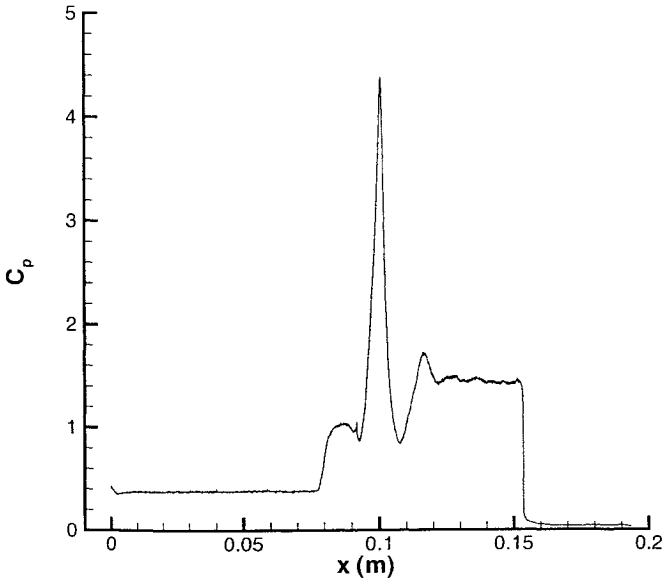

Fig. 10b. Surface profile of pressure coefficient.

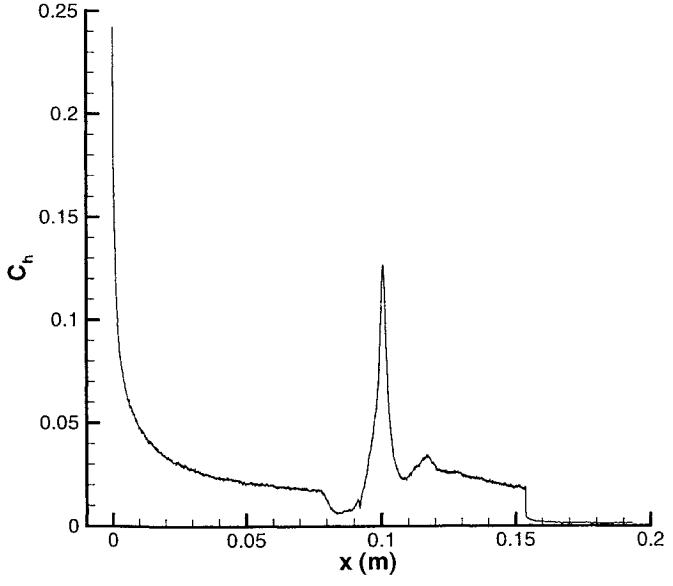

Fig. 10c. Surface profile of heat transfer coefficient.

(c)2001 American Institute of Aeronautics & Astronautics or Published with Permission of Author(s) and/or Author(s)' Sponsoring Organization.

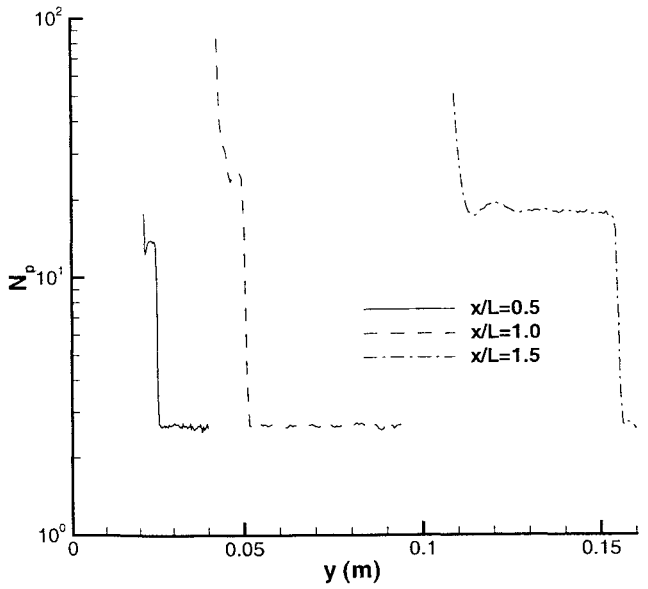

Fig. 11a. Number of particles per cell along three different constant-x coordinates.

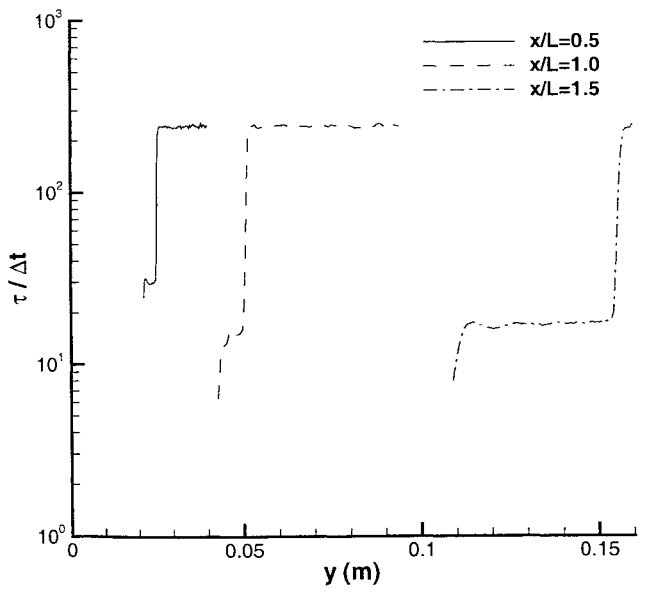

Fig. 11b. Ratio of local mean free time to the simulation time-step along three different constant-x coordinates.

(c)2001 American Institute of Aeronautics & Astronautics or Published with Permission of Author(s) and/or Author(s)' Sponsoring Organization.

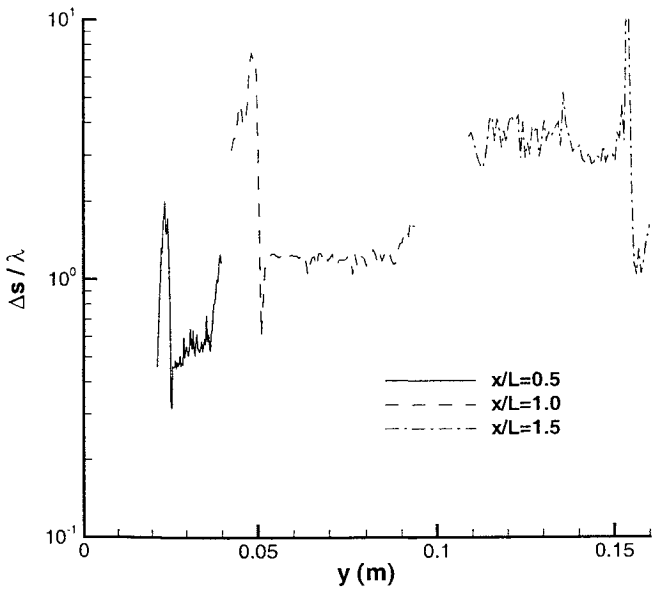

Fig. 11c. Ratio of simulation cell size in direction of maximum gradient to local mean free path along three different constant-x coordinates.

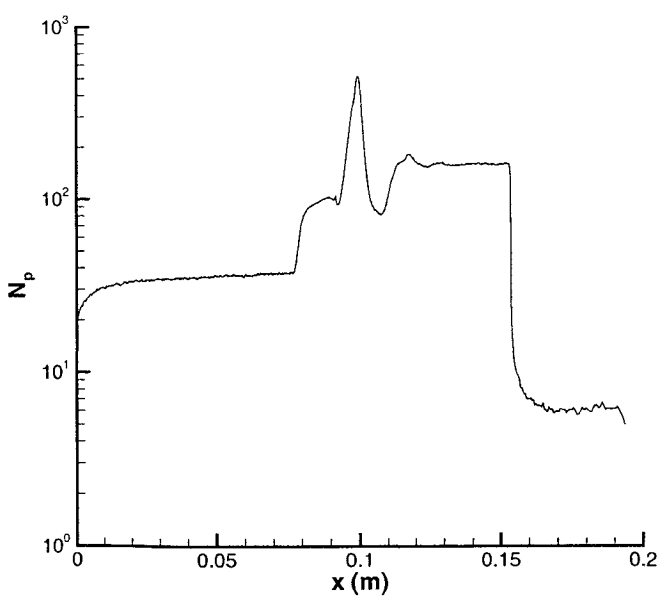

Fig. 12a. Number of particles per cell along the body surface.

(c)2001 American Institute of Aeronautics & Astronautics or Published with Permission of Author(s) and/or Author(s)' Sponsoring Organization.

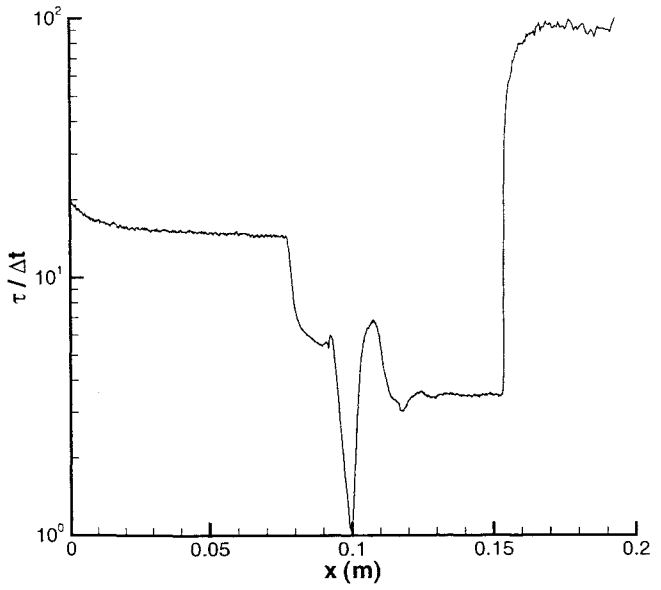

Fig. 12b. Ratio of local mean free time to the simulation time-step along the body surface.

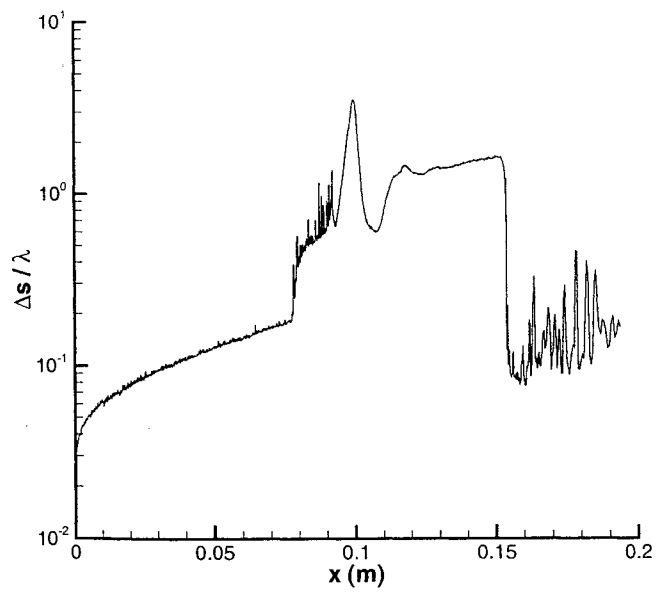

Fig. 12c. Ratio of simulation cell size in direction of maximum gradient to local mean free path along the body surface.

(c)2001 American Institute of Aeronautics & Astronautics or Published with Permission of Author(s) and/or Author(s)' Sponsoring Organization.

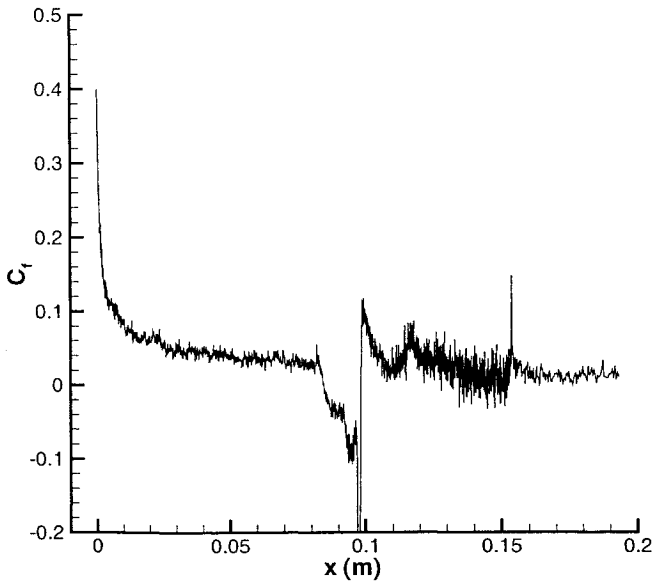

Fig. 13a. Surface profile of friction coefficient.

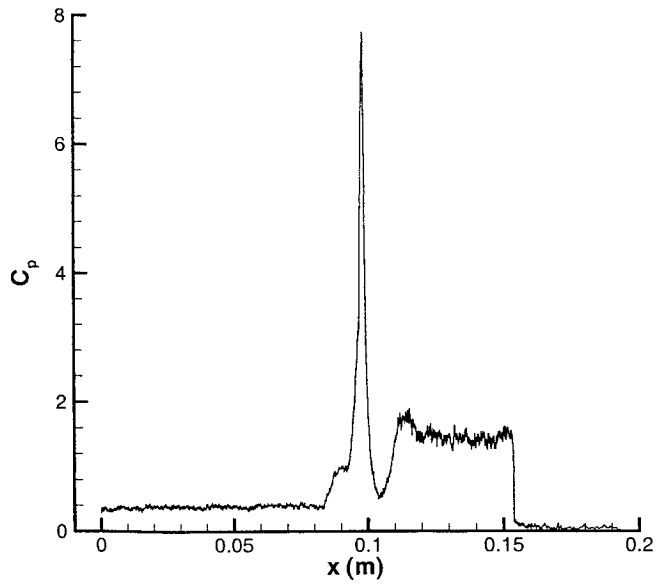

Fig. 13b. Surface profile of pressure coefficient.

(c)2001 American Institute of Aeronautics & Astronautics or Published with Permission of Author(s) and/or Author(s)' Sponsoring Organization.

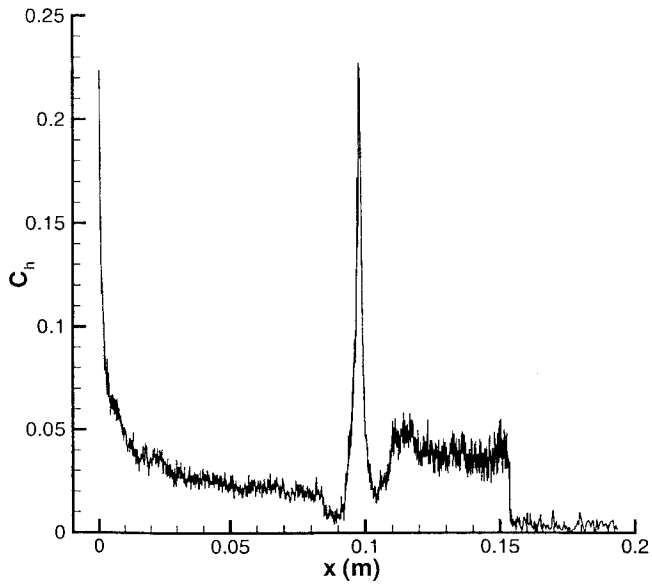

Fig. 13c. Surface profile of heat transfer coefficient.